Quantitative measurement of manganese incorporation into (In,Mn)As islands by resonant x-ray scattering

L. A. B. Marçal,[1] M. S. C. Mazzoni,[1] L. N. Coelho,[2] E. Marega,[3] G. J. Salamo,[4]
R. Magalhães-Paniago,[1] and A. Malachias[1,*]

[1]*Departamento de Física, ICEx, Universidade Federal de Minas Gerais - UFMG, Av. Antonio Carlos, 6627, Belo Horizonte - MG, CEP 30123-970, Brazil*

[2]*Instituto de Física, Universidade de Brasília – UnB, Campus Universitário Darcy Ribeiro, Brasília - DF, CEP 70910-900, Brazil*

[3]*Instituto de Física de São Carlos – Universidade de São Paulo, São Carlos – SP, CEP 13560-970, Brazil*

[4]*Department of Physics, University of Arkansas, Fayetteville, Arkansas 72701, USA*

(Received 2 June 2017; revised manuscript received 20 September 2017; published 5 December 2017)

In this paper we present a method to determine the occupation of Mn ions in epitaxial (In,Mn)As nanostructures by resonant x-ray diffraction near the Mn K-absorption edge, exploiting the dependency of the intensity of both (200) superstructure and the (400) fundamental reflections. The concentrations of Mn atoms on substitutional In sites, as well as on In- and As-interstitial sites, were unambiguously determined. A threshold concentration for the interstitial sites, which are occupied first for low nominal Mn deposition content, was found. Calculations using density-functional theory indicate that a higher occupancy of such sites can be favorable with respect to the occupation of substitutional sites, depending on surface potentials and growth kinetic effects.

DOI: 10.1103/PhysRevB.96.245301

I. INTRODUCTION

In the past decades semiconductor materials with magnetic properties have attracted the attention of the scientific community. Intense effort has been focused on the possibility of combining electronic charge with the spin degree of freedom in a single magnetoelectronic device [1–12]. Particularly interesting physical properties, pointing to a potential use in spintronics, are foreseen for In(Mn)As, as well as Ga(Mn)As [2–5,8,11–17]. Thin films and nanostructures based in these materials are strong candidates to play a substantial role in the next generation of optoelectronic devices and spin-based components, since their lattices may present Mn magnetic ions substituting a fraction of the cations of the original III–V binary compound, which was found to induce local magnetic moment [17]. In such scenario it is crucial to know the density of substitutional and interstitial Mn ions on a given InAs lattice. Mn atoms are expected to modify band-structure properties, since interstitial Mn atoms are double donors, reducing the hole density [6,16,18–20].

Many previous works have been done on nanostructures based on Ga(Mn)As in order to search potentially interesting properties for spintronics applications [5,13,21]. It is known that substitutional Mn does not change the GaAs lattice drastically, in contrast with when it is located in one of the two possible interstitial sites [6,10,18]. X-ray diffraction was used to quantify both the total concentration of Mn atoms on the GaAs lattice and the new lattice parameter after incorporation [19,21,22]. It is known that isolated interstitial Mn atoms reduce the availability of holes in the GaMnAs system [23]. On the other hand, substitutional Mn atoms produce holes that are able to compensate such effect. Since each allocation site impacts on ferromagnetic properties for these structures, it has been reported that ferromagnetism is still observable for some configurations of ternary alloys [23–25].

In this work we have grown In(Mn)As islands through molecular-beam epitaxy (MBE) on GaAs(001) substrates. The amount of Mn codeposited with In and As is varied, leading to distinct Mn incorporation conditions. Resonant (anomalous) synchrotron x-ray diffraction was employed here to provide unambiguously the amount of Mn atoms that enter the islands within each type of lattice site. A threshold for interstitial incorporation of Mn was found, followed by the filling of substitutional sites as the relative Mn/In deposition ratio increases. Density-functional theory (DFT) calculations are employed to address energetic and electronic aspects of Mn incorporation into the InAs lattice.

II. EXPERIMENTAL

The samples studied in this work consist of InMnAs islands grown on semi-insulating GaAs (001) substrates by MBE using a RIBER 32P solid-source apparatus over a high temperature (HT). After oxide desorption a 300-nm GaAs buffer layer was deposited at 580 °C. After the HT GaAs buffer growth, the temperature was lowered to 350 °C under a constant As_4 flux. The $In_{1-x}Mn_xAs$ Quantum dots (QDs) growth follows the usual strained epitaxy within the Stranski-Krastanov growth mode. First, one monolayer (ML) of InAs was deposited and, without any growth interruption, 2.4 ML of $In_{1-x}Mn_xAs$ following the Mn-free material, with $x = 0$, 0.22, and 0.35. The two-dimensional to tridimensional transition takes place at 1.6 ML, with a growth rate set to 0.06 ML/s, using the nominal InAs rate as the reference. The resulting islands were then annealed during 40 s under As_4 flux, which was subsequently interrupted during temperature quench. The $In_{1-x}Mn_xAs$ islands were left uncapped in all samples. The evolution of all processes of the island formation was monitored *in situ* by reflection high-energy electron diffraction. The nominal In:Mn growth ratio was determined by the In/Mn flux rate. Sample A has a 22% Mn composition, while sample B was grown with 35% nominal Mn. A pure InAs sample, called Sample

*Corresponding author: angeloms@fisica.ufmg.br

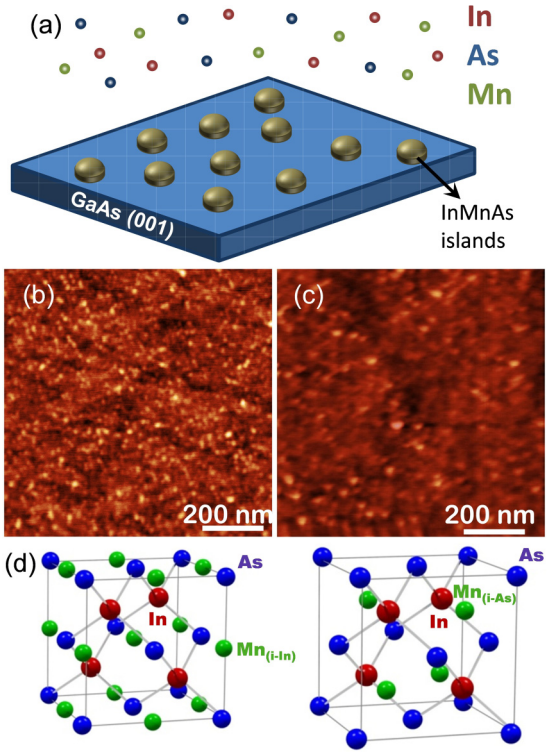

FIG. 1. (a) Representation of the In/Mn/As codeposition during MBE growth of In(Mn)As self-assembled islands. Atomic force microscopy topographic images are shown in (b) and (c) for samples with nominal Mn composition of 22% and 35%, respectively. (d) InAs lattice unit cell (blue and red atoms) with additional green atoms representing the Mn incorporation at interstitial sites, hereafter named In interstitial (i-In) and arsenic interstitial (i-As).

Ref, was also studied. A sketch of the growth of samples A and B is shown in Fig. 1(a).

Atomic force microscopy topography maps were acquired for each sample. The topography of the samples containing Mn is shown in Figs. 1(b) and 1(c) for the lower and higher Mn concentration, respectively. One observes that the islands' density is higher in sample A (1.1×10^{12} islands/cm^2), but structures are bigger on sample B (density 4.0×10^{11} islands/cm^2). For both samples the average island's height was found to be 5.0 nm, with average diameters of 10 nm (sample A) and 18 nm (sample B).

The anomalous x-ray experiments were carried out at grazing-incidence diffraction geometry, mapping the vicinity of the GaAs (200) and (400) reflections at XDS and XRD2 beamlines of the Brazilian Synchrotron Light Laboratory (LNLS). Three different energies used were 6.440, 6.534, and 6.640 keV (the Mn K edge is located at 6.5377 keV). The experiment was performed using a fixed incident angle of 0.4°, at the critical angle of total external reflection. The scattered photons were detected using a Pilatus 100 K detector, which integrates a 2° exit angle. Performing anomalous diffraction in diffuse scattering peaks from self-assembled islands allows the extraction of the atomic content as a function of the local lattice parameter along the lattice gradient observed in these nano-objects. This technique was used in Si:Ge [26,27] and III–V semiconductor islands [28], thin films [19,29], and other systems [30], allowing a concentration sensitivity of 0.5% to a few percent in atomic content, depending on the measurement system (synchrotron source and beamline). Finally, we have also carried out a systematic search for segregated MnAs clusters. No intensity from this binary compound was found at the eight most intense x-ray reflections, indicating that formation (and segregation) of MnAs most likely does not occur.

III. RESULTS

Previous works have indirectly pointed out to the incorporation of Mn atoms at the InAs lattice by measuring the center of mass of diffuse x-ray diffraction near the expected InAs peak position [31]. The observed lattice contraction, which evidenced the presence of Mn atoms, could not be used to quantify the amount of this atomic species incorporated into the islands. In order to quantitatively clarify this question one must derive structure factors for x-ray/electron diffraction, finding out which reflections provide the best contrast.

Similarly to the GaMnAs case, Mn atoms can replace In atoms in the main lattice (substitutional sites), but also enter in interstitial sites, which form new fcc lattices displaced from the In/As original ones. These new lattices are placed at positions which correspond to a displacement of $(-1/8, -1/8, -1/8)$ with respect to the In lattice, constituting the In-interstitial sites (i-In); and at $(-1/8, -1/8, -1/8)$ from the As lattice, constituting the As-interstitial sites (i-As) [19]. These two interstitial lattices are represented in Fig. 1(d) as green dots. Finally, the replacement of As atoms by Mn atoms is energetically unfavorable and was not observed experimentally in both InMnAs and GaMnAs compounds [6].

The quantification of the Mn concentration for each site can be carried out by exploring the structure factor dependency of fundamental and superstructure reflections using x-ray energies near the Mn K edge. For fundamental (strong) reflections such as (220), (400), and (620), the scattered intensity I^{fund} calculated for the unit cell with both interstitial sides is given by [19]

$$I^{\text{fund}} = I_0|f_{\text{In}} + f_{\text{As}} + C_s(f_{\text{Mn}} - f_{\text{In}}) + f_{\text{Mn}}(C_{i-\text{As}} + C_{i-\text{In}})|^2, \quad (1)$$

where I_0 is a constant that depends on setup parameters (incident photon flux, illumination footprint, etc.), C_s, $C_{i-\text{As}}$, and $C_{i-\text{In}}$ are the concentration of the substitutional and both interstitial Mn sites, respectively, and f_{In}, f_{As}, and f_{Mn} are the atomic scattering factors of In, As, and Mn. Some of the plus signs of Eq. (1) are replaced by minus signs in the scattered intensity I^{sup} of superstructure reflections such as (200) and (420), which is then given by

$$I^{\text{sup}} = I_0|f_{\text{In}} - f_{\text{As}} + C_s(f_{\text{Mn}} - f_{\text{In}}) + f_{\text{Mn}}(C_{i-\text{As}} - C_{i-\text{In}})|^2. \quad (2)$$

For x-ray energies that are near an absorption edge of a specific element (anomalous conditions) the dispersion (f') and absorption (f'') factors of the atomic scattering factor change drastically, as shown in Fig. 2(a). The quantitative results for f' and f'' shown in this figure are retrieved by measuring fluorescence directly from the nominally 35% Mn

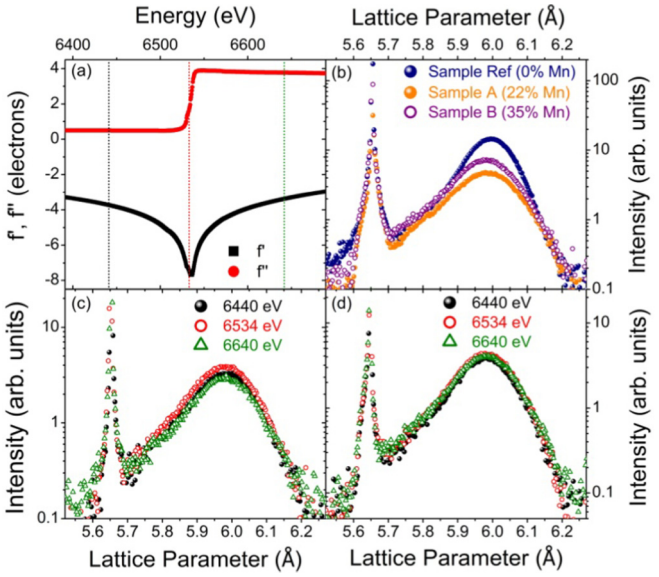

FIG. 2. (a) Dispersion (f') and absorption (f'') atomic scattering factor corrections near the Mn K edge used in this work (measurements/calculations follow Ref. [31]). (b) Longitudinal scans near the GaAs (200) in-plane reflection for samples grown with different nominal Mn content. The broad In(Mn)As peak slightly shifts its maximum toward smaller lattice parameter as more Mn is added to the system. From the analysis of its intensity in different energies around the Mn K edge, shown in the anomalous measurements of panels (c) (sample A) and (d) (sample B), the substitutional Mn concentration and the difference between interstitial concentrations can be found.

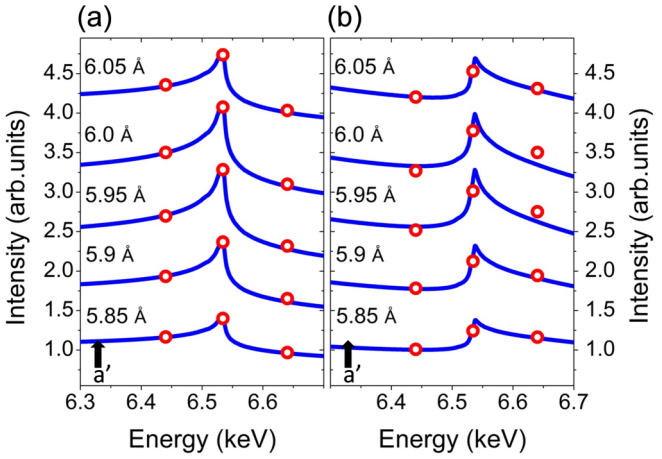

FIG. 3. Fits to the diffracted intensity near the (200) reflection at selected local lattice parameters near the In(Mn)As broad peak for samples (a) A and (b) B. Here we represent the dependency of the scattering intensity with the energy of the incident photons as solid lines, which must fit the experimental data (open dots) retrieved from each of the three energies used.

sample (sample B) within an energy range that comprises the Mn K edge and performing a Kramers-Kronig calculation, according to Ref. [31]. Measuring diffraction in selected energies near the Mn K edge allows for distinct scattering responses from each possible site in the InMnAs structure. Making use of two reflections (a fundamental and a superstructure reflection), it is possible to retrieve the Mn content for each of the three Mn sites discussed previously.

A first glimpse of the effect of adding Mn atoms to the diffraction of In(Mn)As islands in nonresonant and resonant conditions is shown by the longitudinal scans of Figs. 2(b)–2(d). In these figures the reciprocal space position near the GaAs (200) reflection was directly converted into local lattice parameter. One observes that besides the GaAs narrow peak a diffuse scattering arises, due to the In(Mn)As lattice of the islands. From Fig. 2(b) one observes that the addition of Mn atoms shifts the diffuse hump of island diffraction–which has a peak at 6.00 Å for the reference InAs sample–toward slightly smaller lattice parameter values (5.99 Å for sample A and 5.98 Å for sample B). This indirect evidence of Mn incorporation is better understood at anomalous conditions. Figures 2(c) and 2(d) show longitudinal scans for samples A and B at the three distinct photon energies.

Intensity contrast dependency on the photon energy is well observed for sample A but not clearly seen for similar measurements on sample B. The poor contrast in this latter case [Fig. 2(d), sample B] could, in a quick observation, lead to the conclusion that Mn is not being incorporated at the InAs lattice, since the presence of Mn atoms in one of the described sites is enough to generate anomalous intensity variations. From Eq. (2) one perceives that the term related to substitutional Mn atoms contributes negatively for the measured intensity, as well as the term for the In-interstitial position. However, at the Mn K edge, the first term (substitutional Mn) becomes more negative, while the second one (i-In) changes its value, approaching zero. The term corresponding to the As-interstitial position is positive and its value reduces at the Mn edge. The interplay between behaviors for each of the three different Mn sites explains why it is possible to find low contrast around the absorption edge, even having considerable amounts of Mn incorporated at the sample.

In order to quantify such behavior, Eqs. (1) and (2) are solved as a function of each of the Mn concentration variables and the intensity I_0 (normalization constant) for each of the measured energies. The problem becomes better determined (and nonambiguous) with the use of three energies and two reflections. This allows for a fit to the experimental data by varying C_s, $C_{i-\mathrm{As}}$, and $C_{i-\mathrm{In}}$. Some of these fits are shown in Fig. 3 for samples A and B using intensities of the (200) reflection. At this reflection a clear distinction of the substitutional C_s and interstitial difference $(C_{i-\mathrm{As}} - C_{i-\mathrm{In}})$ terms is obtained. One notices that the intensity for selected local lattice parameters in Fig. 3(a) is larger at energies below the Mn K edge than at higher energies. This trend is modified for the results of Fig. 3(b). While the fits of the first case (sample A) can be carried out by using zero values for C_s and a negative value for $(C_{i-\mathrm{As}} - C_{i-\mathrm{In}})$, both terms must differ from zero in order to fit the data retrieved for sample B. Particularly, we find $C_s = 0$ and $C_{i-\mathrm{As}} - C_{i-\mathrm{In}} = -0.3$ for sample A and $C_s = 0.4$ and $C_{i-\mathrm{As}} - C_{i-\mathrm{In}} = -0.3$ for sample B. These values correspond to the average concentration retrieved for in-plane lattice parameters ranging from 5.95 to 6.05 Å.

A removal of possible ambiguations of the Mn content of each interstitial site is provided by the analysis of the (400)

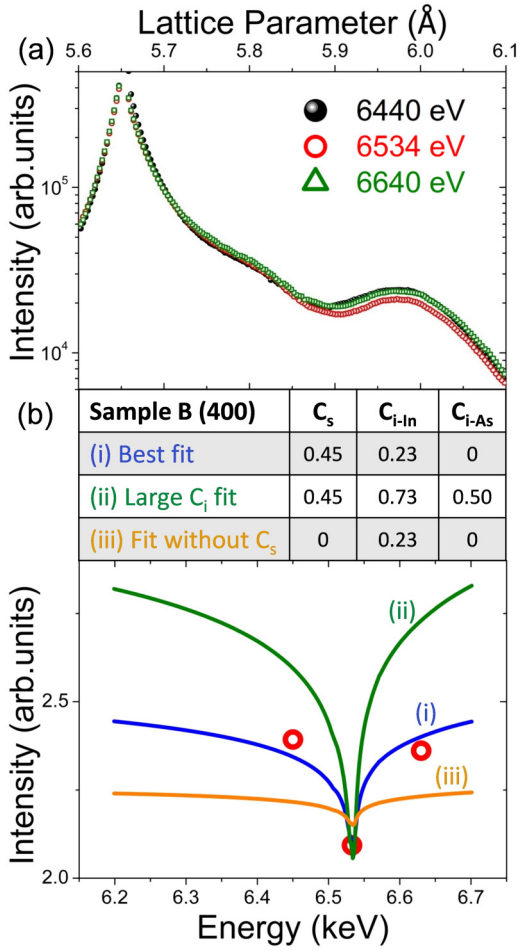

FIG. 4. (a) Longitudinal scans carried out on sample B near the GaAs (400) reflection, using three different energies for the incident photons. (b) Quantitative results from fits with different combinations of C_s, $C_{i-\mathrm{In}}$, and $C_{i-\mathrm{As}}$, shown in (c), for the experimental data retrieved from the curves shown in panel (a) for $a' = 5.98$ Å. The distinct possibilities explored in this figure represent graphically the uniqueness of the solution of C_i and C_s values, providing the specific Mn content on the interstitial In and As sites, which were entangled in the results from the (200) reflection. The use of large values of C_i [still respecting the difference obtained from the (200) data], or a different C_s does not fit the experimental results.

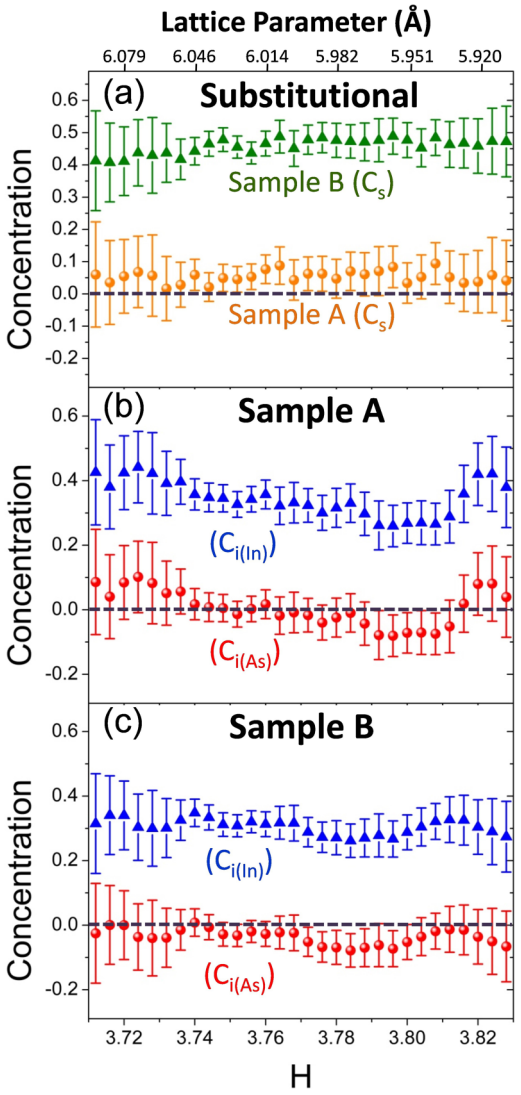

FIG. 5. Mn concentrations for samples A and B retrieved at the vicinity of the In(Mn)As peak for substitutional Mn (a) and the In-interstitial and the As-interstitial sites for samples A [panel (b)] and B [panel (c)].

reflection, shown in Fig. 4. In the longitudinal scans of Fig. 4(a) one can observe the anomalous contrast measured at sample B near $a' = 5.98$ Å as the energy changes near the Mn K edge. The analysis of such contrast can be quickly performed at this point by fixing the C_s value retrieved at the (200) reflection, as well as the difference $(C_{i-\mathrm{As}} - C_{i-\mathrm{In}})$. In fact, the robustness of our results was also corroborated by leaving the C_s value free to change over the fit procedure, which rapidly converges to the retrieved amount of substitutional Mn from the (200) reflection. Hence, the correct determination of $C_{i-\mathrm{As}}$ and $C_{i-\mathrm{In}}$ is carried out by fitting the intensity profile at each lattice parameter probed along the longitudinal scans for the three energies. One example, for a fixed local lattice with $a' = 5.98$ Å, is shown in Fig. 4(b). A unique solution is found for $C_{i-\mathrm{As}} = 0$ and $C_{i-\mathrm{In}} = 0.23$. Trial fits with other values which also respect the $(C_{i-\mathrm{As}} - C_{i-\mathrm{In}})$ difference or take into consideration $C_s = 0$ fail in reaching the correct intensity values for the measured energies. After the refinement of compositions using the (200) reflection as a reference condition to the (400) refinement, we have performed an independent corefinement of all data. The composition retrieved was the same, which supports the robustness of the method used. The fitting procedure along all measured local lattice parameters and the three energies was carried out for samples A and B. The final composition at the In(Mn)As islands is depicted in Fig. 5.

IV. DISCUSSION

Once the best parameters are calculated using both (200) and (400) reflections, it is possible to separate unambiguously the percentage of Mn allocated at each of the two possible interstitial sites and the substitutional one for the lattice

parameters along the In(Mn)As peak. Our results show that for sample A almost no Mn atoms substitute the In in the lattice, and only in the In-interstitial site an amount of about 35% is occupied. A different scenario is observed for sample B where, still, the As-interstitial site remains unoccupied (zero Mn concentration) and the In interstitial, presenting the same 35% occupation observed in sample A. However, at sample B the substitutional Mn concentration is much larger, reaching 45% replacement of the original In-lattice sites. These results are depicted in Fig. 5(a), showing the distinct amount of substitutional Mn found for the samples with 22% (A) and 35% (B) nominal Mn concentration. Figures 5(b) and 5(c) show for samples A and B, respectively, the amount of In-interstitial sites and As-interstitial sites occupied by the Mn atoms. The similarities of these figures suggest that the Mn starts to fill the In-interstitial sites until a saturation threshold is reached. After such saturation limit the substitutional sites, which probably present a higher activation barrier, become the favorable target for the incoming Mn atoms. The As-interstitial sites occupation seem to be highly unfavorable, indicating that due to its expected chemical coordination a much larger energy barrier needs to be overcome in order to place Mn atoms there.

A theoretical analysis of this issue was performed by means of spin-density-functional theory [32,33] (DFT) within the SIESTA implementation [34], which includes the use of norm-conserving Troullier-Martins pseudopotentials [35] in the Kleinman-Bylander factorized form [36] and a numerical basis set composed of finite range pseudoatomic orbitals. The generalized gradient approximation with the modified Perdew-Burke-Ernzerhof (PBE) parametrization of Y. Zhang and W. Yang [37] was chosen to determine the exchange-correlation functional. All coordinates in our geometric models were relaxed until the maximum force component in each atom was less than 0.026 eV/Å. Using this analysis we address the energetic aspects of the Mn incorporation into the InAs structure as well as the electronic structure of the resulting doped compound.

An atomistic description of an InAs-Mn island with 10-nm diameter and 5.0-nm height is not affordable within an *ab initio* scheme. However, since we are seeking general trends rather than a quantitative analysis, we adopted a simplified model based on an initial cubic InAs supercell comprising 64 atoms (two replications of the primitive cell in each direction). The pseudomorphic out-of plane lattice expansion observed at the islands, which is found to be near 10% (with respect to the GaAs lattice) as shown by the out-of-plane (002) x-ray reflection depicted in Fig. 6(a), was also considered for the calculations. Figure 6(b) shows the In(Mn)As supercell, in which periodic boundary conditions were imposed in the three directions. The lengths of the lattice vectors in the x, y, and z directions were fixed in 12, 12, and 12.93 Å (15% expansion with respect to GaAs), respectively, to mimic the measured dimensions in our experiments. As an example, the middle and lower panels of Fig. 6(b) show the initial and final geometries, respectively, for eight interstitial Mn atoms randomly placed into the InAs matrix.

We begin our discussion with the energetic aspects involved in the doping process. It is well established in previous theoretical works that a single Mn atom incorporates preferably in an In substitutional site. For instance, there has been reported

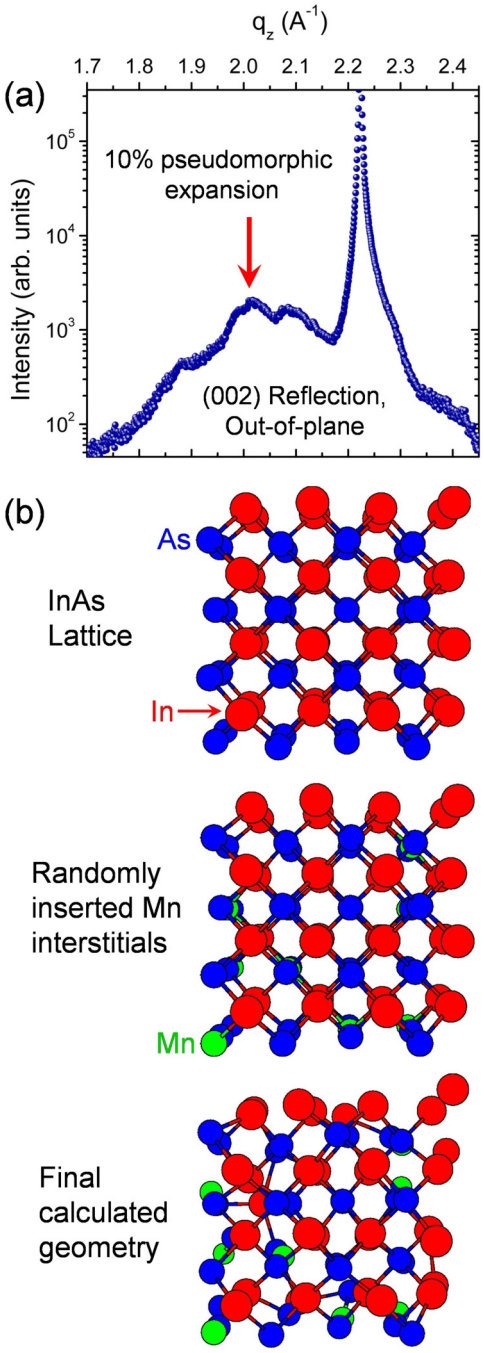

FIG. 6. (a) Longitudinal scan near the GaAs x-ray (002) reflection (sharp peak at $q_z = 2.22$ Å^{-1}), showing the diffuse scattering from the InAs islands of sample B (centered at a lattice parameter 10% larger than the GaAs lattice). (b) Geometric model for a InAs supercell with two replications in each direction, without Mn (upper panel) and at the initial and final states with Mn doping the interstitial sites (middle and lower panel, respectively). Blue, red, and green spheres represent As, In, and Mn atoms, respectively.

[38] a formation energy difference of 1.11 eV favoring it with respect to an interstitial site in which the Mn is first neighbor to four As atoms. It is therefore intriguing why we observe a large amount (35% of available sites) of interstitial Mn atoms in both A and B samples. Even more intriguing is the i-In site, which is 0.48 eV less favorable compared to the i-As

site according to our total energy calculations for a single Mn interstitial, the one observed in our experiments.

Interestingly, our theoretical results suggest a trend which may be related to this phenomenology. Using the models previously mentioned, we performed DFT calculations to determine formation energies for structures containing $n = 1$, 2, 4, and 8 Mn atoms, with Mn atoms placed in randomly chosen sites, according to expressions (3) and (4):

$$(E_F)_{\text{int}} = E_T(\text{InAsMn}_n) - E_T(\text{InAs}) - n\mu_{\text{Mn}}, \quad (3)$$

$$(E_F)_{\text{sub}} = E_T(\text{InAsMn}_n) + n\mu_{\text{In}} - E_T(\text{InAs}) - n\mu_{\text{Mn}}, \quad (4)$$

in which E_T is the total energy directly derived from the bulk DFT calculation; μ_{Mn} and μ_{In} are the chemical potentials for Mn and In, respectively. The relevant quantity in our reasoning is the difference per number of Mn atoms (n) between the formation energies in interstitial and substitutional configurations, $\Delta E_F/n$, shown in expression (5):

$$\frac{\Delta E_F}{n} = \frac{(E_T)_{\text{int}} - (E_T)_{\text{sub}}}{n} - \mu_{\text{In}}, \quad (5)$$

in which μ_{In} is determined from a bulk In calculation in a body-centered tetragonal phase.

The results, depicted in Fig. 7(a), show a monotonic decreasing behavior of the energetic cost associated with the formation of interstitial structures compared to substitutional ones. The choice of In chemical potential is not unique, which means that we cannot pinpoint what value of n is related to a sign change in $\Delta E_F/n$. Also, it was not our goal to find the lowest energy configurations for each n, which would be a formidable task beyond the scope of the present work. However, the calculations can definitely establish that the stability of interstitial doping increases with the number of Mn atoms: Indeed, Fig. 7(a) shows that from $n = 1$ to 8 the lower bound for energetic gain for doping in interstitial sites in comparison with the substitutional case is at least 0.78 eV, a result that may be ascribed to structural relaxations originating from local distortions, as it can be seen in Fig. 6(b), and the enhancement of Mn-Mn interactions. It is still important to address the problem of the relative stability between the two distinct interstitial configurations, since, as mentioned before, the i-As site for a single Mn leads to a structure 0.48 eV lower in energy. To check if this result is preserved for a large amount of Mn atoms, we performed an additional calculation for eight Mn atoms placed in i-As interstitial sites. The retrieved result indicates an inversion: In this condition it is the i-In structure which is lower in energy, with a calculated total energy difference of 0.30 eV. Therefore, we once more detected an energetic trend favoring i-In interstitial Mn incorporation for large Mn amounts.

Concerning the electronic properties, we found that the incorporation of Mn atoms in the concentrations considered in the present work tends to close the energy gap in our bulk doping models. This is evident in the electronic band structure shown in Fig. 7(b) for a single interstitial Mn (i-In site) in the 2×2×2 InAs supercell. Similar features are present in the calculations for $n = 2$, 4, and 8 Mn atoms. The absence of band gap with the inclusion of Mn atoms is in agreement with

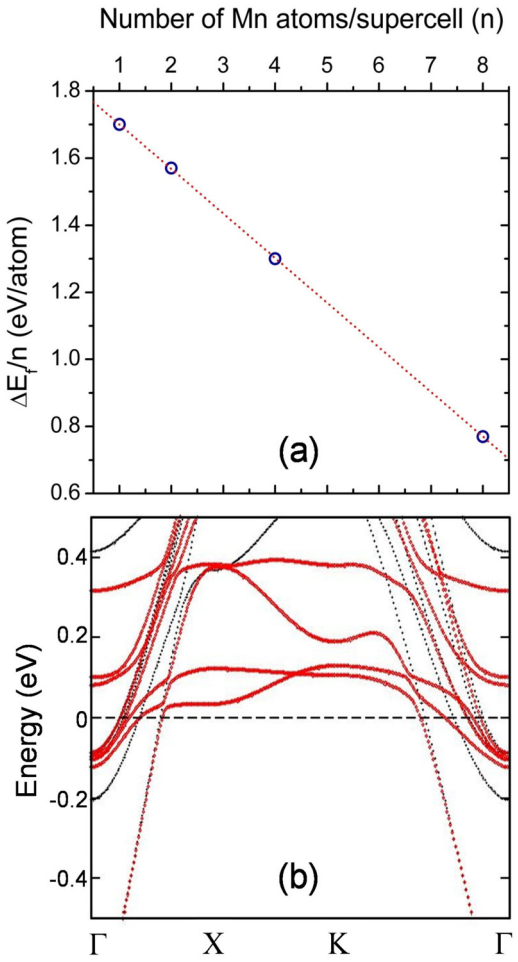

FIG. 7. (a) Difference in formation energy of In(Mn)As per Mn atom (n) between interstitial and substitutional doping configurations as a function of n. The dotted straight line is solely a guide to the eyes. (b) Electronic band structure for a single Mn atom in the simulated In(Mn)As supercell, placed in an In-interstitial (i-In) site. The Fermi level is set to zero, and red and black lines distinguish the two spin components. X and K represent the points (1,0,0) and (1,1,0), respectively, in units of π/a ($a = 12$ Å).

the lack of photoluminescence observed in capped In(Mn)As quantum dot samples.

Finally, although a clear contrast is observed between DFT calculations and the retrieved Mn content from anomalous diffraction results, a more complete qualitative scenario has to be established on the basis of growth conditions. DFT calculations are based in thermal equilibrium conditions, which do not take into account the surface kinetic mechanisms of Mn incorporation into InAs islands. Such process, which takes place far from the thermodynamic equilibrium during the MBE growth of islands, is probably responsible for the rich Mn content on In-interstitial sites. The contact between experiments and the simulation framework explored here is found on the increasingly lower energy of additional Mn atoms at the In-interstitial sites as the Mn content becomes larger in such condition. We believe the growth dynamics used allows a sufficient supply of Mn atoms that are incorporated in In-interstitial sites at a large rate, probably due to surface

strain or surface-driven processes, helping to reduce activation barriers and the final overall system energy to a point where this type of incorporation is stabilized.

V. CONCLUSION

Our experimental results using three photon energies near the Mn K-absorption edge and comparing the intensity contrast in fundamental and superstructure x-ray reflections show, unambiguously, that Mn atoms can be incorporated at the InAs lattice of self-assembled islands. Interstitial In sites are initially occupied for low Mn nominal deposition content, while the presence of Mn atoms in substitutional In sites is only detected after an approximately 35% In-interstitial Mn-filling threshold. Such result may be a consequence of the island surface potentials and Mn incorporation kinetic mechanisms, which can be favored by the strain relaxation at the In(Mn)As island surface. DFT simulations were also carried out. Despite their inherent thermal equilibrium character, these simulations show that, for increasing Mn content on interstitial In sites, the energy for insertion of additional Mn atoms at other interstitial sites on the resulting deformed lattice decreases.

ACKNOWLEDGMENT

The authors acknowledge FAPEMIG, FAPESP (Grant No. 2013/07276-1), CAPES, and CNPq for financial support. Beamtime was granted on XRD2 and XDS beamlines by LNLS/MCTI.

[1] H. Munekata, H. Ohno, S. Von Molnar, A. Segmüller, L. L. Chang, and L. Esaki, Phys. Rev. Lett. **63**, 1849 (1989).
[2] H. Ohno, H. Munekata, T. Penney, S. Von Molnár, and L. L. Chang, Phys. Rev. Lett. **68**, 2664 (1992).
[3] S. Koshihara, A. Oiwa, M. Hirasawa, S. Katsumoto, Y. Iye, C. Urano, H. Takagi, and H. Munekata, Phys. Rev. Lett. **78**, 4617 (1997).
[4] H. Akai, Phys. Rev. Lett. **81**, 3002 (1998).
[5] J. Blinowski and P. Kacman, Phys. Rev. B **67**, 121204 (2003).
[6] J. Mašek, J. Kudrnovský, and F. Máca, Phys. Rev. B **67**, 153203 (2003).
[7] G. D. Sanders, Y. Sun, F. V. Kyrychenko, C. J. Stanton, G. A. Khodaparast, M. A. Zudov, J. Kono, Y. H. Matsuda, N. Miura, and H. Munekata, Phys. Rev. B **68**, 165205 (2003).
[8] D. Chiba, Y. Sato, T. Kita, F. Matsukura, and H. Ohno, Phys. Rev. Lett. **93**, 216602 (2004).
[9] J. Mašek and F. Máca, Phys. Rev. B **69**, 165212 (2004).
[10] J. Sadowski and J. Z. Domagala, Phys. Rev. B **69**, 075206 (2004).
[11] J. Wang, C. Sun, J. Kono, A. Oiwa, H. Munekata, A. Cywiński, and L. J. Sham, Phys. Rev. Lett. **95**, 167401 (2005).
[12] G. A. Khodaparast, Y. H. Matsuda, D. Saha, G. D. Sanders, C. J. Stanton, H. Saito, S. Takeyama, T. R. Merritt, C. Feeser, B. W. Wessels, X. Liu, and J. Furdyna, Phys. Rev. B **88**, 235204 (2013).
[13] A. H. MacDonald, P. Schiffer, and N. Samarth, Nat. Mater. **4**, 195 (2005).
[14] O. V. Vikhrova, Y. A. Danilov, B. N. Zvonkov, A. V. Kudrin, V. V. Podol'Skiĭ, Y. N. Drozdov, M. V. Sapozhnikov, C. Moura, M. I. Vasilevskiy, and M. P. Temiryazeva, Phys. Solid State **50**, 52 (2008).
[15] J. Novák, I. Vávra, Z. Križanová, S. Hasenöhrl, J. Šoltýs, M. Reiffers, and P. Štrichovanec, Appl. Surf. Sci. **256**, 5672 (2010).
[16] J. A. Peters and B. W. Wessels, Phys. E **42**, 1447 (2010).
[17] I. T. Yoon, S. Lee, Y. Shon, S. W. Lee, and T. W. Kang, J. Phys. Chem. Solids **72**, 181 (2011).
[18] I. Kuryliszyn-Kudelska, J. Z. Domagala, T. Wojtowicz, X. Liu, E. Lusakowska, W. Dobrowolski, and J. K. Furdyna, J. Appl. Phys. **95**, 603 (2004).
[19] V. Holý, X. Martí, L. Horák, O. Caha, V. Novák, M. Cukr, and T. U. Schülli, Appl. Phys. Lett. **97**, 181913 (2010).
[20] F. A. Ferri, L. N. Coelho, V. P. Kunets, G. J. Salamo, and E. Marega, J. Appl. Phys. **112**, 034317 (2012).
[21] I. Frymark and G. Kowalski, J. Phys. D: Appl. Phys. **38**, A160 (2005).
[22] L. Horák, Z. Sobáň, and V. Holý, J. Phys.: Condens. Matter **22**, 296009 (2010).
[23] P. Mahadevan and A. Zunger, Phys. Rev. B **68**, 075202 (2003).
[24] K. M. Yu, W. Walukiewicz, T. Wojtowicz, I. Kuryliszyn, X. Liu, Y. Sasaki, and J. K. Furdyna, Phys. Rev. B **65**, 201303(R) (2002).
[25] F. Máca and J. Mašek, Phys. Rev. B **65**, 235209 (2002).
[26] M. Stoffel, A. Malachias, A. Rastelli, T. H. Metzger, and O. G. Schmidt, Appl. Phys. Lett. **94**, 253114 (2009).
[27] A. Malachias, M. Stoffel, M. Schmidbauer, T. Ü. Schulli, G. Medeiros-Ribeiro, O. G. Schmidt, R. Magalhães-Paniago, and T. H. Metzger, Phys. Rev. B **82**, 035307 (2010).
[28] M. Sztucki, T. U. Schülli, T. H. Metzger, E. Beham, D. Schuh, and V. Chamard, Superlattices Microstruct. **36**, 11 (2004).
[29] C. Lefevre, A. Thomasson, F. Roulland, V. Favre-Nicolin, Y. Joly, Y. Wakabayashi, G. Versini, S. Barre, C. Leuvrey, A. Demchenko, N. Boudet, and N. Viart, J. Appl. Crystallogr. **49**, 1308 (2016).
[30] J. Coraux, B. Amstatt, J. A. Budagovski, E. Bellet-Amalric, J. Rouvière, V. Favre-Nicolin, M. G. Proietti, H. Renevier, and B. Daudin, Phys. Rev. B **74**, 195302 (2006).
[31] Y. Waseda, *Anomalous X-Ray Scattering for Materials Characterization* (Springer-Verlag, Berlin, 2002).
[32] P. Hohenberg and W. Kohn, Phys. Rev. **136**, B864 (1964).
[33] W. Kohn and L. J. Sham, Phys. Rev. **140**, A1133 (1965).
[34] J. M. Soler, E. Artacho, J. D. Gale, A. García, J. Junquera, P. Ordejón, and D. Sánchez-Portal, J. Phys.: Condens. Matter **14**, 2745 (2002).
[35] N. Troullier and J. L. Martins, Phys. Rev. B **43**, 1993 (1991).
[36] L. Kleinman and D. M. Bylander, Phys. Rev. Lett. **48**, 1425 (1982).
[37] Y. Zhang and W. Yang, Phys. Rev. Lett. **80**, 890 (1998).
[38] J. T. Arantes, G. M. Dalpian, and A. Fazzio, Phys. Rev. B **78**, 045402 (2008).